Langmuir

Article

pubs.acs.org/Langmuir

Electrically Tunable Wetting Defects Characterized by a Simple Capillary Force Sensor

Dieter 't Mannetje,[†] Arun Banpurkar,[†,‡] Helmer Koppelman,[†] Michel H. G. Duits,[†] Dirk van den Ende,[†] and Frieder Mugele*[,†]

[†]Physics of Complex Fluids and MESA+ Institute for Nanotechnology, University of Twente, P.O. Box 217, 7500 AE Enschede, The Netherlands

[‡]Department of Physics, University of Pune, Pune-411007, India

Supporting Information

ABSTRACT: We present a concept of a wetting defect of continuously variable strength based on electrowetting, along with a capillary force sensor adapted for the characterization of macroscopically heterogeneous surfaces. Patterned electrodes submerged under an insulating layer are used to generate potential wells for drops of electrically conductive liquids on the solid surface, with a well depth that scales with the diameter of the drop and square of the applied alternating (AC) voltage. We characterize the strength of the electrowetting trap and the hysteretic motion of the drop along the surface, using a simple force sensor based on optical imaging of a thin bendable capillary. A force resolution of approximately 0.1 μN is achieved.

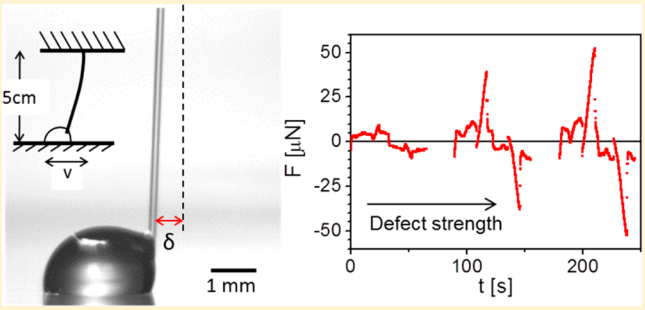

INTRODUCTION

Drops on solid surfaces are a ubiquitous sight, encountered among others on windscreens of cars in the rain, on airplane wings, and in printing, coating, and cleaning technology. Frequently, it is difficult to remove these drops because they are held back by heterogeneities on the surface. In particular, for small drops, gravity and drag by an airflow may not be strong enough to overcome the pinning forces. In other applications, such as microfluidic lab-on-a-chip systems,[1,2] spray painting, and pesticide deposition,[3] the opposite may be desirable, the sticking of drops to surfaces at certain locations. The surface heterogeneities can be either of topographic or of chemical nature. If their characteristic lateral scale is small compared to the size of the drop, microscopic random pinning forces ensue that lead to contact angle hysteresis.[4,5] If their lateral scale is comparable to the drop size, however, they give rise to localized discrete pinning sites, to which the entire drop can adhere. Such discrete pinning sites give rise to a complex energy landscape, in which the drop can adjust its shape to reach some, usually local, minimum of its energy. The evolution of the drop shape under external forcing is usually characterized by sequences of discrete transitions of the morphology of the entire drop.[6,7] Depending on their size, shape, and profile, such localized defects can lead to very strong pinning forces,[8,9] and drops may even break apart if forced to depin.

Characterizing pinning due to localized defects is also much more difficult than in the case of microscopic random pinning forces. In the latter case, contact angle hysteresis measurements have been used extensively to characterize the strength of the heterogeneity. These measurements are based, for example, on drop shape analysis or drop sliding on inclined planes.[10−15] Such measurements provide the mean value of microscopic pinning forces averaged over the length scale of the drop. A meaningful interpretation of such measurements requires a separation of length scales with microscopic pinning forces that are homogeneous on the global scale of the drop. Mesoscopic heterogeneity leads to substantial distortions of the three-phase contact line and complex interactions between adjacent defects.[10−13] In this case, the roughness of the contact line provides a suitable measure of the defect strength. For well-ordered defects, mesoscopic heterogeneity can also result in globally anisotropic wetting properties of the surface, as, for instance, in the extreme case of surfaces with one-dimensional wettability patterns.[14] Individual localized wetting defects on the global scale of the drop can usually not be analyzed with the aforementioned techniques. For this kind of heterogeneity, in principle, a full three-dimensional characterization of the drop surface would be required to understand the pinning forces. However, this approach is generally rather tedious and restricted to numerical studies[15] or to very specific geometries as, for instance, in Klingner and Mugele.[16] On the other hand, a very detailed description of energy landscapes and precise drop morphologies is often not required. From a practical

Received: April 25, 2013
Revised: June 28, 2013
Published: July 5, 2013

   dx.doi.org/10.1021/la4015724 | Langmuir 2013, 29, 9944−9949

perspective, a global measure such as the maximum retention force is often sufficient to characterize a defect.

In this Article, we present a novel technique to design localized wetting defects of continuously variable strength based on electrowetting (EW), as well as a capillary force sensor to characterize them. The tunable EW defects are based on patterned substrates submerged under an insulating layer as usual in EW. We develop a physical model based on energy minimization to characterize the strength of the tunable EW defects and compare the results to experimental measurements using our capillary force sensor. The latter makes use of the bending of a thin capillary.[17−19] Optical imaging of the deflection of the capillary in a conventional contact angle goniometer setup is used to measure the forces experienced by a drop attached to the lower end of the capillary as it is dragged across the surface of interest.

EXPERIMENTAL SECTION

We first describe the capillary force sensor and its operation on macroscopically homogeneous surfaces with a well-defined contact angle hysteresis. The force sensor consists of a capillary glass tube with a typical length of several centimeters and an (outer) diameter of order 100 μm (see Figure 1a). A wide range of such capillaries are commercially available from Vitrocom Inc. The bending stiffness of the capillaries is calibrated by mounting them horizontally and by imaging the deflection upon attachment of aqueous drops of varying sizes; these drops are created by pumping water through the capillary, so the spring constant is for a filled capillary. For a typical capillary of 5 cm and an outer diameter of 170 μm (wall thickness 20 μm), we obtain a spring constant of k_c = 16.3 mN/m (see Figure 1b). During operation of the sensor, the capillary is mounted vertically, and the drop is again created by pumping liquid through it. It is imaged from the side along with the drop and the surface with a long-distance variable zoom lens with a magnification ranging from 0.65 to 6 times. The substrate of interest is mounted on a motorized linear translation stage with a maximum translation range of 50 mm with a maximum speed of 0.5 mm/s. The deflection δ (see Figure 1a) of the capillary is extracted from the video frames using a straightforward image processing routine written in Matlab. For typical zoom settings, the resulting sensitivity is approximately 50 nN/pixel, depending on the spring constant of the capillary. In practice, mechanical vibrations and/or air flow typically limit the force resolution of our setup to approximately 100 nN. Mounting the entire setup on an inverted microscope allows for additional bottom view imaging in the case of transparent substrates. This enables a precise characterization of the drop−substrate interface.

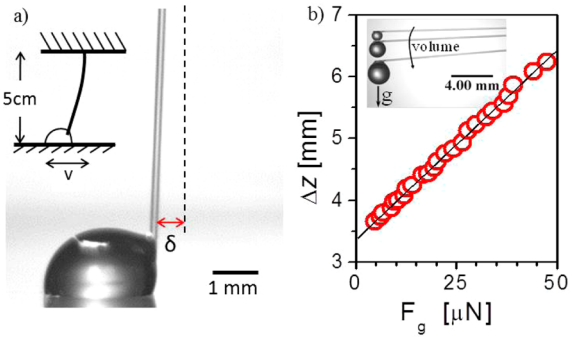

Figure 1. (a) Schematic setup (inset) of the device and side view snapshot of a drop being dragged across the surface. (b) Capillary deflection versus drop weight yielding calibration of the spring constant of the capillary (here: 16.3 mN/m).

The substrates in our experiments consist, unless otherwise noted, of an adhesive tape (Scotch Pressure Sensitive, consisting of polypropylene and a glue layer) glued onto an ITO (indium tin oxide) coated glass substrate. Prior to the experiments, we coat this surface with a thin film of silicone oil (viscosity: 5 mPa s) to achieve a very low contact angle hysteresis of 3° (θ_A = 95 ± 2°, θ_R = 92 ± 2° as measured by a contact angle goniometer). The oil layer is applied by gently rubbing a dust-free tissue soaked in silicone oil over the surface, followed by doing the same with a dry tissue. Consistent with the specifications of the manufacturer, we find an effective thickness d of the compound glue/polypropylene/oil layer of 39 μm at a dielectric constant ε = 2. This value is determined by measuring the EW response $\cos\theta(U) = \cos\theta_y + \eta$ of the system following standard procedures.[20] Here, $\eta = \varepsilon\varepsilon_0 U^2/2\sigma d$ is the dimensionless EW number, with $\varepsilon\varepsilon_0$ being the dielectric permittivity of the substrate. The EW defect is generated by etching a gap of width a into an ITO layer prior to applying the adhesive tape (see below in Figure 4). An alternate (AC) voltage (frequency: 1 kHz; root mean square (RMS) voltage U = 0−375 V) is applied between the resulting two separated electrodes. This corresponds to a maximum EW number of η_{max} = 0.44.

RESULTS AND DISCUSSION

To test and calibrate the device, we measure the force upon periodically translating a drop of (originally) 30 μL back and forth along a homogeneous substrate (i.e., without EW defect) over a distance of approximately ±2 cm. The force curves shown in Figure 2a display well-defined plateau values of the force upon dragging in one direction and the opposite force upon moving in the opposite direction. Typically the data display a slight but continuous decrease during the first few cycles of drop motion. We attribute this effect to a gradual evolution of the surface during the first cycles of wetting, possibly in combination with evaporation effects; we find that the radius of the drop reduces by about 2% over the course of the experiment. If we replot the data as a function of the displacement x of the drop with respect to the solid surface, we

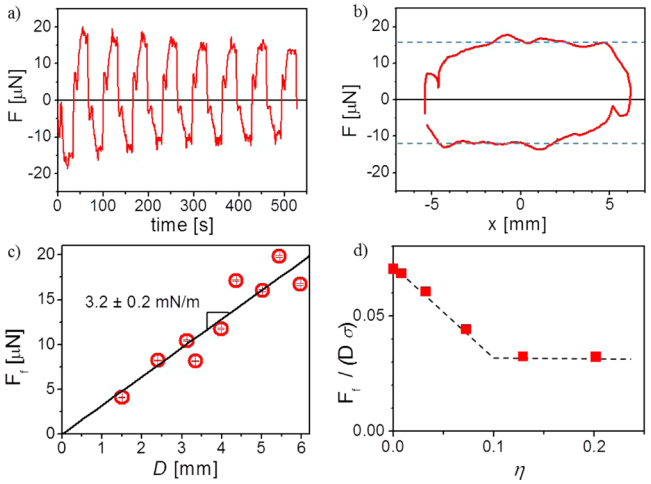

Figure 2. Hysteresis force on homogeneous substrate. (a) Force versus time upon translating the stage back and forth. Positive and negative force values correspond to drops moving toward right and left, respectively (drop volume, 30 μL; substrate, oil-impregnated polypropylene tape). (b) Force versus drop position on the surface (extracted from data in (a)). After reversal of the sliding direction, plateau values of friction force (dashed lines) are only reached once the capillary has traversed the drop. (c) Hysteresis force (plateau values of friction force) versus drop diameter. (d) Hysteresis force versus electrowetting number on Teflon film. Dashed line is a guide to the eye indicating the expected decrease in hysteresis with increasing AC voltage for small η. Drop volume: 5 μL.

dx.doi.org/10.1021/la4015724 | Langmuir 2013, 29, 9944−9949

obtain a hysteresis loop; see Figure 2b. The hysteresis loop displays well-defined plateaus for the phases of continuous dragging both in the positive and in the negative direction. During these phases of well-defined pulling, the capillary adheres to the drop at some fixed location close to the foremost apex of the advancing contact line approximately 100−200 μm above the substrate (see Figure 1). Upon reversing the translation stage, the capillary changes its position with respect to the drop until it eventually ends up in a symmetric position close to the opposite contact line. The trajectory of the capillary as it moves from one stable pulling position to the other can be complex and involve bending perpendicular to the pulling direction. The width of this poorly defined region (from about −5.5 to −3 mm for the positive force branch and +5.5 to 3 mm for the negative force branch in Figure 2b) corresponds to the width of the drop. (Because the drop morphology changes, relating the forces extracted from the deflection of the needle to drop-sample friction forces would require a full characterization and analysis of the actual drop shape at any moment during this phase, which is outside our present scope of developing a simple sensor. We therefore disregard these transient phases in our further analysis.) To avoid any bias between forward and backward motion, we determine the friction force F_f of the sliding drop as one-half the height of the hysteresis loop between the two dashed lines in Figure 2b. Figure 2c shows this force for a series of drops of various base diameter D between 1 and 6 mm. The force is found to increase linearly with the diameter, as expected on the basis of earlier work on sliding drops:[3,21−25]

$$F_f = c\sigma w\Delta \cos\theta \quad (1)$$

Here, σ is the surface tension of the drop and w is the width of the drop perpendicular to the direction of motion. From our bottom view images, we find that the drop−substrate interface is not appreciably deformed under the conditions of the present experiments such that $w = D = 2R$. c is a prefactor of order 1 that depends on the details of the drop shape (see El Sherbini 2006[25] for an overview and references there). For a hardly deformed half-spherical drop, Dussan and Chow found $c = 1$.[21] For the present surface, the contact angle hysteresis is $\Delta \cos\theta = 0.05$, as determined by conventional contact angle goniometry. Using the surface tension of water, we hence expect a relation $F_f = c\ w\ 3.7 \times 10^{-3}$ mN/m, suggesting a value of $c \approx 0.85$ for the present experiments. We note, however, that the exact value is rather sensitive to small errors in the measurement of the advancing and receding contact angle, which only differ by 3 ± 1° in the present experiments (see above). Given the uncertainty of the hysteresis measurement, we conclude that the data are consistent with $c = 1$ within error and do not allow one to distinguish between the competing expressions described in El Sherbini et al.[25]

Notwithstanding the uncertainty regarding the exact value of c, it is worthwhile to note here that our data in Figure 2c clearly confirm the linear increase of the friction force with the drop diameter as predicted in eq 1, in agreement with similar capillary-based sliding drop results in the literature.[19] This linear relation has been challenged recently by Tadmor and co-workers,[26−28] who argued that the approximate linearity observed in many drop sliding experiments on inclined planes is an artifact caused by the simultaneous variation of the tangential and normal components of the gravitational force in inclined plane experiments, and that the true retention force should be independent of the drop size. Our measurements clearly avoid that artifact. Yet, we still recover the linear relation reported in the inclined plane experiments.

In Figure 2d, we show another test demonstrating the sensitivity of our device. In this case, we applied a varying AC voltage U between the ITO electrodes submerged under the insulating polymer layer, functioning as two coplanar electrodes.[29] Conventional contact angle hysteresis measurements under AC-EW have shown that the contact angle hysteresis is effectively reduced under these conditions, because the alternating electrostatic force pulling on the contact line helps the drop to overcome microscopic pinning forces.[23,30] For small voltages, the reduction of the contact angle hysteresis is expected to scale linearly with the EW-number. As shown in Figure 2d, this effect can indeed be detected by our capillary force sensor. (Note that this experiment was performed on a PTFE (Teflon) film with thickness $d = 10$ μm that provides a larger initial hysteresis ($\theta_a = 117 \pm 2°$, $\theta_r = 84 \pm 2°$) than the oil-lubricated adhesive tape samples.)

In Figure 3, we provide another example of a force measurement, now on a superhydrophobic surface consisting of a plasma-treated SU-8 surface with nanoroughness similar to the work of Gnanappa et al.[31] By reducing the drop to just a small cap protruding from the capillary, we can limit the diameter of the drop−substrate interface to a few tens of micrometers. In this case, the friction force is reduced to just 1 μN. We expect that this approach will be of considerable interest to probe the pinning and depinning of drops at individual pillars on microstructured superhydrophobic surfaces.

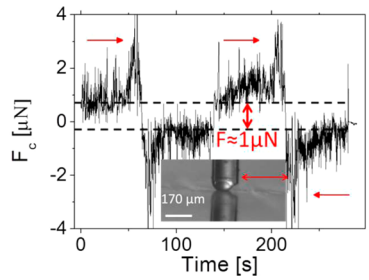

Figure 3. Friction force versus time upon dragging a micrometer-sized drop over a superhydrophobic surface with nanoscale roughness illustrating force resolution of <1 μN.

Having established the sensitivity of our capillary sensor, we now consider the tunable EW defects and their properties. As explained above, the specific EW defect consists of two insulator-covered electrodes separated by a small gap of width a. The drop then forms two parallel plate capacitors $C_{1/2}(x) = \varepsilon\varepsilon_0 A_{1/2}(x)/2d$ with the two underlying electrodes (see Figure 4a and b). Here, $A_{1/2}(x)$ denotes the overlap area between the drop and the respective electrode, which depends on the position x of the center of mass of the drop with respect to the center of the gap. As the drop moves from one electrode to the other, $A_{1,2}$ varies from 0 to A (and vice versa), while the sum $A_1 + A_2 = A = \pi R^2$ remains constant, if we neglect the finite value of a. The areas can be conveniently expressed as a function of the angle φ as $A_{1,2} = R^2(\pi/2 \pm (\varphi + \sin(2\varphi)/2))$, where φ is given by $x = R \sin\varphi$ (see Figure 4a). Being electrically conductive, the drop capacitively couples the two electrodes such that the entire system can be represented by a simple equivalent circuit with the two capacitors $C_1(x)$ and $C_2(x)$ in series. The potential of the electrically floating drop adjusts

dx.doi.org/10.1021/la4015724 | Langmuir 2013, 29, 9944−9949

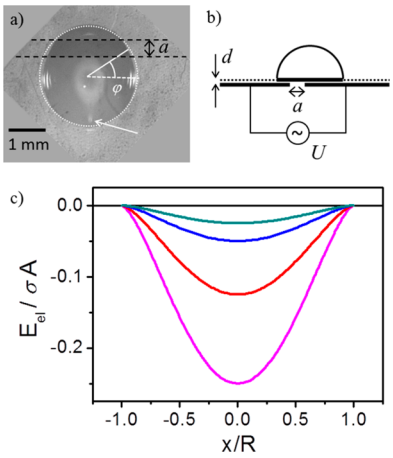

Figure 4. Drop on an EW trap. (a) Bottom view of the drop being pulled out of the trap by a capillary (position indicated by arrow). The slightly darker horizontal band (marked by dashed lines) close to the top shows the gap between the electrodes. Dashed circle indicates effective circle. (b) Schematic side view of a circular drop passing an EW trap. (c) Electrostatic energy in the trap versus the lateral drop position in normalized units for increasing EW number of 0.1, 0.2, 0.5, and 1 (top to bottom).

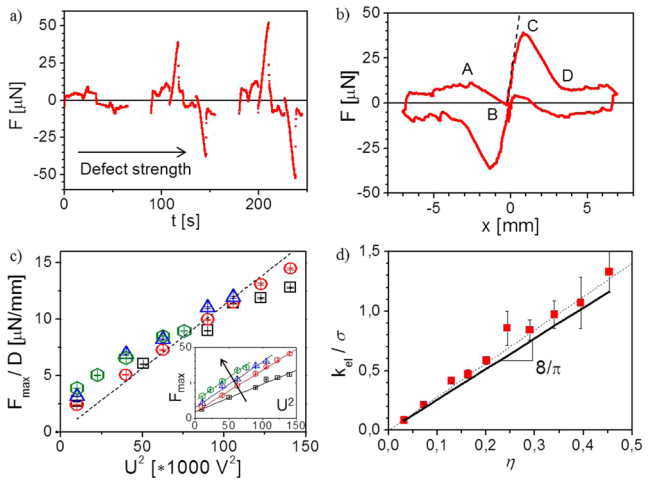

Figure 5. (color online) Drop trapping at EW defect. (a) Force versus time upon passing the trap in the forward and backward direction for U = 100, 300, 375 V (left to right; drop volume: 10 μL). (b) Force versus drop position displaying mechanical instabilities upon entering and leaving the trap for the 375 V data from (a). Dashed line: Linear approximation for small deflections yielding the electric trap stiffness k_{el}. (c) Maximum trapping force versus square of applied voltage for various drop sizes increasing along arrow in inset (black, 5; red, 10; blue, 15; green, 20 μL). Inset: Raw force data in μN versus U^2 in units of [1000 V^2]. Main panel: Normalized force versus U^2. Dashed line: Expected maximum force (eq 3). (d) Normalized trap stiffness versus EW number. Symbols: Experimental data, now grouped according to EW number. Solid line: Prediction of eq 4. Dotted line: Modified eq 4 including finite gap width.

itself accordingly such that the voltage between the drop and the electrodes 1 and 2 is given by $\Delta U_{1/2}(x) = C_{2/1}(C_1 + C_2)U$, respectively. The resulting electrostatic contribution to the free energy of the entire system then reads:

$$E_{el} = -\frac{1}{2}C(x)U^2 = -\sigma\eta A \cdot g(\varphi) \tag{2}$$

where $C(x) = C_1(x)C_2(x)/(C_1(x) + C_2(x))$ is the resulting capacitance that depends on the drop position x. For $x < R$, $C(x)$ can be conveniently expressed in terms of the dimensionless function $g(\varphi) = ((\pi/2)^2 - (\varphi + \sin(2\varphi)/2)^2)/\pi^2$ using elementary geometric relations. This results in a symmetric potential well with a depth $E_{min} = -A\sigma\eta/4$ as shown in Figure 4c. The corresponding electrostatic trap force is given by

$$f_{el} = -\frac{dE_{el}}{dx} = \frac{4\sigma\eta R}{\pi}\cos\varphi(\varphi + \cos\varphi \sin\varphi) \tag{3}$$

The trap force reaches its maximum at value $f_{el,max} \approx 1.16\ \sigma R\eta$ at a drop position $x_{max}/R \approx 0.67$. Because η is of order 0.1−1, eq 3 implies that the maximum pinning force of the EW trap is comparable to a chemical wetting defect with a contact angle contrast of several tens of degrees. The stiffness of the trap (linearized for small deflections) is

$$k_{el} = df_{el}/dx_{x=0} = 8\sigma\eta/\pi \tag{4}$$

For the surface tension of water (σ = 72 mN/m), this results in a stiffness $k_{el} \approx 180\ \eta$ mN/m. Note that, unlike the energy and the force, the spring constant turns out to be independent of the drop size. (A small correction of order a/R appears if the finite gap width a is taken into account.)

Figure 5 shows force curves measured for drops moving back and forth across the EW defect. Next to the plateau values of the force, time traces for a single drop recorded at voltages of 100, 300, and 375 V (Figure 5a, left to right) show sharp peaks as the drops are being pulled out of the potential well formed by the defect. Video sequences (see Supporting Information) also show that the drop displays instabilities both upon entering and upon leaving the trap. Plotting the measured force versus the drop position, we recover the same constant friction force as discussed above when the drop is far away from the defect ($|x| > 3$ mm). As the drop reaches the edge of the defect (point A in Figure 5b), it is dragged into the potential well and "jumps" to position B. As the stage is moved further, the drop is gradually pulled out of the trap leading to an initially linear increase in the force as indicated by the dashed line. The slope of this line indicates the stiffness k_{el} of the trap. For larger deflections, the force increases more gradually and eventually reaches a maximum. Upon approaching the maximum force (point C), the drop slightly deforms, as can be seen in Figure 4a and the Supporting Information. The maximum deformation in the present experiments is approximately $L/w|_{max} \approx 1.1$, with L the length of the drop along the direction of translation. At point C, the drop again becomes unstable and snaps rapidly out of the trap toward point D. From point D onward, the drop is again dragged smoothly across the surface at a constant force until the direction of the stage is reversed. The appearance of instabilities, such as the snap-off, is typical for mechanical systems with competing spring constants where a softer spring (here: the capillary) is used to probe the force of a stiffer spring (the EW defect). Because k_{el} can be tuned externally, we can tune the absence or presence of the mechanical instability by adjusting the strength of the defect with respect to the capillary.

To quantitatively characterize the EW defect, we extract both the maximum force F_{max} and the spring constant k_{el} of the trap for a series of drop volumes ranging from 5 to 20 μL. As expected, F_{max} indeed increases linearly with U^2 (see Figure 5c). Moreover, F_{max} scales linearly with the diameter of the drop, as expected on the basis of eq 3. Experimentally, we find a slightly weaker voltage-dependence of F_{max} than predicted by the

dx.doi.org/10.1021/la4015724 | Langmuir 2013, 29, 9944−9949

model. We attribute this deviation to the finite deformation of the drop within the trap. Figure 5d shows the trap stiffness k_{el} (normalized by the surface tension), as extracted from the initial slope of the force curves, for drops ranging from 5 to 20 μL. Within the experimental resolution, the data follow a linear relation independent of the size of the drop. The solid line represents the expectation based on eq 4 using the independently measured EW response of the drop. In this case, the slight underestimation of the slope is presumably caused by the neglect of the finite gap width a in our simplified model. Reintroducing $a \approx 500$ μm into our model, we find an increase of the slope by approximately 10%, in very good agreement with the experimental findings (see dashed line in Figure 5d). The simple electrostatic model thus describes the behavior of the trap rather well.

CONCLUSION

In summary, our simple capillary force sensor is able to detect capillary forces caused by contact angle hysteresis on homogeneously rough surfaces as well as localized pinning forces due to wetting defects with a resolution of order 0.1 μN. We anticipate that the resolution may ultimately be further increased by improving vibration isolation, protection from air currents, as well as higher resolution optical imaging. Our results also demonstrate that EW defects are a flexible tool for the trapping and release of drops. Our measurements demonstrate that simple electrostatic considerations provide a quantitative description of the tool. The maximum pinning forces are of the same order of magnitude as surface forces. We anticipate in particular fruitful applications in the area of drop-based microfluidics with channels, where traps of arbitrary shapes can be generated using specific lithographically designed electrode patterns to control and guide drops in desired directions.

ASSOCIATED CONTENT

Supporting Information

Movie of a 10 μL drop being dragged over a 375 V defect by a capillary. This material is available free of charge via the Internet at http://pubs.acs.org.

AUTHOR INFORMATION

Corresponding Author

*E-mail: f.mugele@utwente.nl.

Notes

The authors declare no competing financial interest.

ACKNOWLEDGMENTS

This work is part of the research programme "Contact Line Control during Wetting and Dewetting" (CLC) of the "Stichting voor Fundamenteel Onderzoek der Materie (FOM)", which is financially supported by the "Nederlandse Organisatie voor Wetenschappelijk Onderzoek (NWO)". The CLC programme is cofinanced by ASML and Océ.

REFERENCES

(1) Dangla, R.; Lee, S.; Baroud, C. N. Trapping microfluidic drops in wells of surface energy. *Phys. Rev. Lett.* **2011**, *107*, 124501.
(2) Seemann, R.; Brinkmann, M.; Pfohl, T.; Herminghaus, S. Droplet based microfluidics. *Rep. Prog. Phys.* **2012**, *75*, 016601.
(3) Furmidge, C. G. Studies at phase interfaces. 1. Sliding of liquid drops on solid surfaces and a theory for spray retention. *J. Colloid Sci.* **1962**, *17*, 309.
(4) Gennes, P.-G. d.; Brochard-Wyart, F.; Quéré, D. *Capillarity and Wetting Phenomena: Drops, Bubbles, Pearls, Waves*; Springer: New York, 2004; p xv, 291 p.
(5) Johnson, R. E.; Dettre, R. H. Contact angle hysteresis. III. Study of an idealized heterogeneous surface. *J. Phys. Chem.* **1964**, *68*, 1744−1750.
(6) Lenz, P.; Lipowsky, R. Morphological transitions of wetting layers on structured surfaces. *Phys. Rev. Lett.* **1998**, *80*, 1920−1923.
(7) Herminghaus, S.; Gau, H.; Monch, W. Artificial liquid microstructures. *Adv. Mater.* **1999**, *11*, 1393−1395.
(8) Joanny, J. F.; Degennes, P. G. A model for contact-angle hysteresis. *J. Chem. Phys.* **1984**, *81*, 552−562.
(9) Oliver, J. F.; Huh, C.; Mason, S. G. Resistance to spreading of liquids by sharp edges. *J. Colloid Interface Sci.* **1977**, *59*, 568−581.
(10) Delon, G.; Fermigier, M.; Snoeijer, J. H.; Andreotti, B. Relaxation of a dewetting contact line. Part 2. Experiments. *J. Fluid Mech.* **2008**, *604*, 55−75.
(11) Cubaud, T.; Fermigier, M. Faceted drops on heterogeneous surfaces. *Europhys. Lett.* **2001**, *55*, 239.
(12) Reyssat, M.; Quere, D. Contact angle hysteresis generated by strong dilute defects. *J. Phys. Chem. B* **2009**, *113*, 3906−3909.
(13) Nadkarni, G. D.; Garoff, S. An investigation of microscopic aspects of contact-angle hysteresis - Pinning of the contact line on a single defect. *Europhys. Lett.* **1992**, *20*, 523−528.
(14) Bliznyuk, O.; Jansen, H. P.; Kooij, E. S.; Poelsema, B. Initial spreading kinetics of high-viscosity droplets on anisotropic surfaces. *Langmuir* **2010**, *26*, 6328−6334.
(15) Semprebon, C.; Herminghaus, S.; Brinkmann, M. Advancing modes on regularly patterned substrates. *Soft Matter* **2012**, *8*, 6301−6309.
(16) Klingner, A.; Mugele, F. Electrowetting-induced morphological transitions of fluid microstructures. *J. Appl. Phys.* **2004**, *95*, 2918−2920.
(17) Suda, H.; Yamada, S. Force measurements for the movement of a water drop on a surface with a surface tension gradient. *Langmuir* **2002**, *19*, 529−531.
(18) Lagubeau, G.; Le Merrer, M.; Clanet, C.; Quere, D. Leidenfrost on a ratchet. *Nat. Phys.* **2011**, *7*, 395−398.
(19) Pilat, D. W.; Papadopoulos, P.; Schäffel, D.; Vollmer, D.; Berger, R.; Butt, H. J. Dynamic measurement of the force required to move a liquid drop on a solid surface. *Langmuir* **2012**.
(20) Mugele, F.; Baret, J. C. Electrowetting: From basics to applications. *J. Phys.: Condens. Matter* **2005**, *17*, R705−R774.
(21) Dussan, E. B.; Chow, R. T. P. On the ability of drops or bubbles to stick to non-horizontal surfaces of solids. *J. Fluid Mech.* **1983**, *137*, 1−29.
(22) Bikerman, J. J. Sliding of drops from surfaces of different roughnesses. *J. Colloid Sci.* **1950**, *5*, 349−359.
(23) 't Mannetje, D. J. C. M.; Murade, C. U.; van den Ende, D.; Mugele, F. Electrically assisted drop sliding on inclined planes. *Appl. Phys. Lett.* **2011**, *98*, 014101−014103.
(24) Extrand, C. W.; Kumagai, Y. Liquid-drops on an inclined plane - the relation between contact angles, drop shape, and retentive force. *J. Colloid Interface Sci.* **1995**, *170*, 515−521.
(25) ElSherbini, A.; Jacobi, A. Retention forces and contact angles for critical liquid drops on non-horizontal surfaces. *J. Colloid Interface Sci.* **2006**, *299*, 841−849.
(26) Tadmor, R. Approaches in wetting phenomena. *Soft Matter* **2011**, *7*, 1577−1580.
(27) Tadmor, R.; Bahadur, P.; Leh, A.; N'guessan, H. E.; Jaini, R.; Dang, L. Measurement of lateral adhesion forces at the interface between a liquid drop and a substrate. *Phys. Rev. Lett.* **2009**, *103*, 266101.
(28) Tadmor, R. Line energy and the relation between advancing, receding, and Young contact angles. *Langmuir* **2004**, *20*, 7659−7664.
(29) Sen, P.; Kim, C. J. Capillary spreading dynamics of electrowetted sessile droplets in air. *Langmuir* **2009**, *25*, 4302−4305.

(30) Li, F.; Mugele, F. How to make sticky surfaces slippery: Contact angle hysteresis in electrowetting with alternating voltage. *Appl. Phys. Lett.* **2008**, *92*, 2441081−2441083.
(31) Gnanappa, A. K.; Gogolides, E.; Evangelista, F.; Riepen, M. Contact line dynamics of a superhydrophobic surface: application for immersion lithography. *Microfluid. Nanofluid.* **2011**, *10*, 1351−1357.